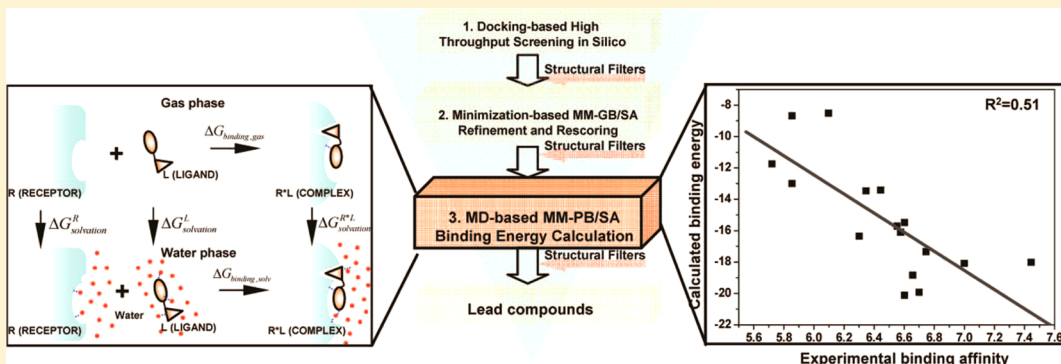


# Evaluation and Application of MD-PB/SA in Structure-Based Hierarchical Virtual Screening

Ran Cao, Niu Huang, and Yanli Wang\*

National Institute of Biological Sciences, Beijing, No. 7 Science Park Road, Zhongguancun Life Science Park, Beijing, 102206, China

Supporting Information



**ABSTRACT:** Molecular dynamics (MD) based molecular mechanics Poisson–Boltzmann and surface area (MM-PB/SA) calculation (MD-PB/SA) has been widely used to estimate binding free energies for receptor–ligand complexes. While numerous reports have focused on assessing accuracy and efficiency, fewer studies have paid attention to performance in lead discovery. In the present study, we report a critical evaluation of MD-PB/SA in hierarchical virtual screening (HVS) both theoretically and practically. It is shown that based on native poses, MD-PB/SA could be well applied to predict the relative binding energy for both congeneric and diverse ligands for different protein targets. However, there is a limitation for MD-PB/SA to distinguish the native pose of one ligand from the artificial pose of another when a huge difference exists between two molecules. By combining a physics-based scoring function with a knowledge-based structural filter, we improve the predictability and validate the practical use of MD-PB/SA in lead discovery by identifying novel inhibitors of p38 MAP kinase. We also expand our study to other protein targets such as HIV-1 RT and NA to assess the general validity of MD-PB/SA.

## INTRODUCTION

Molecular dynamics (MD) simulation based molecular mechanics Poisson–Boltzmann and surface area (MM-PB/SA), here called MD-PB/SA for convenience, is a free energy estimating method in which one can perform MD simulation with an explicit solvent model and collect a set of representative structures (snapshots) and, then, conduct calculations for each different energy term to obtain the ensemble averaged free energy (Formula 1).<sup>1</sup>

$$\bar{G} = \bar{E}_{\text{MM}} + \bar{G}_{\text{PBSA}} - T\bar{S}_{\text{MM}} \quad (1)$$

$$\bar{E}_{\text{MM}} = \bar{E}_{\text{bond}} + \bar{E}_{\text{angle}} + \bar{E}_{\text{tors}} + \bar{E}_{\text{vdW}} + \bar{E}_{\text{elec}} \quad (2)$$

where  $\bar{E}_{\text{MM}}$  is the average molecular mechanical energy including bond, angle, torsion, van der Waals, and electrostatic terms (Formula 2),  $\bar{G}_{\text{PBSA}}$  is the solvation free energy calculated with a finite difference solution of Poisson–Boltzmann equation and an estimate of the nonpolar free energy with a surface area-based term,  $-T\bar{S}_{\text{MM}}$  is the solute entropy estimated with normal-mode analysis.

Since the first introduction by Kollman in 2000,<sup>2</sup> MD-PB/SA has been widely used in the study of interaction between

receptor and small molecular ligand.<sup>3–7</sup> Among the earliest work, Kollman et al. reproduced experimental binding free energies ( $\Delta G_{\text{bind}}$ ) with MD-PB/SA calculation for series of ligands of avidin and HIV-1 RT respectively,<sup>8,9</sup> with a mean-squared error typically lower than 3 kcal/mol.<sup>10</sup> Later, McCammon et al. also obtained a good correlation between experimental data ( $\text{pIC}_{50}$ ) and calculated binding free energies ( $\Delta G_{\text{bind}}$ ) for numerous ligands of CDK2, on which basis they further designed novel potent CDK2 inhibitor.<sup>11</sup> When combining MD-PB/SA with molecular docking, it was shown that the enrichment significantly improved.<sup>12,13</sup>

Despite the impressive achievements, there still exist problems in MD-PB/SA. Pearlman has reported a study of 16 congeneric ligands of p38 MAP kinase.<sup>14</sup> As a result, an inferior performance was surprisingly found for MD-PB/SA compared with thermodynamic integration (TI), one window free energy grid (OWFEG), and even molecular docking. On this basis, it is suggested that MD-PB/SA protocol could not be trusted when attempting to predict the binding behavior for

Received: April 1, 2014



ACS Publications

© XXXX American Chemical Society

A

dx.doi.org/10.1021/ci5003203 | J. Chem. Inf. Model. XXXX, XXX, XXX–XXX

small molecular ligands, which caught our attention. What's more, while numerous studies focused on assessing accuracy and efficiency,<sup>15,16</sup> fewer prospective studies explored the potential of this powerful method in lead discovery, especially in the practice of high throughput virtual screening without any prior knowledge about potential binders. Sippl et al. performed MD-PB/SA calculation to evaluate candidates identified by molecular docking and observed a significant correlation between binding free energy and experimental inhibition. However, such work were generally limited to the analogue and lacks confidence referring to high diversity in large library.<sup>17</sup> Zhang et al. recently reported the identification of sumoylation activating enzyme 1 inhibitors with MD-PB/SA integrated virtual screening protocol,<sup>18</sup> but there is a lack of detailed discussion about the computational results, especially for MD-PB/SA. Besides of these, other work from peers also made progress. Chen et al. combined multiple protocols including molecular docking, a pharmacophore model, and MD-PB/SA to identify potent AChE inhibitors with a novel scaffold.<sup>19</sup> Venken et al. also demonstrated that the virtual screening approach with adapted MD-PB/SA methodology can improve the accuracy of energy calculations and holds promise in the discovery of HIV-1 gp41 FP inhibitors.<sup>20</sup>

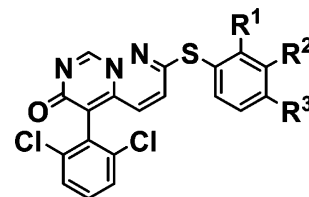
In the present study, we reported a critical evaluation of MD-PB/SA in the framework of hierarchical virtual screening (HVS), both theoretically and practically. With congeneric and diverse data sets of p38 MAP kinase ligands, we clarified the effects of solvent model and starting poses on the energy estimation. It was found that on the basis of native binding pose, MD-PB/SA could be well applied to predict relative binding energy for different ligands. However, there's limitation in distinguishing the native pose of one ligand from the artificial pose of another, especially when the huge difference exists between two molecules. By combining a physics-based scoring function with a knowledge-based structural filter, we improved the predictability and validated the practical use in lead discovery by identifying novel inhibitors of p38 MAP kinase. At last, we expanded our study to other protein targets such like HIV-1 RT and NA to examine the general utility of MD-PB/SA.

## RESULTS AND DISCUSSION

**System Setup.** In MD-PB/SA calculation, the most time-consuming part is MD based sampling with an explicit solvent model. To enhance the efficiency, one widely used strategy is replacing periodic boundary conditions (PBCs) with a non-PBC water cap model which surrounds the interested site.<sup>9,14</sup> However, a small solvent model like water cap could lead to artificial effects, such as a vacuum in the binding site. According to our previous work, it is found that a water sphere with a radius of 30 Å centered on the ligand can achieve good balance between efficiency and accuracy. In addition, we also added additional water into the emerging vacuum after each equilibration of solvents. The same operation was repeated at least three times, and then followed with a production run, which further ensures the prevention of a vacuum in the binding site.

**Study of p38 Congeneric Data Set.** We first studied 16 cognates of p38 MAP kinase inhibitor (Table 1), which has been reported by Pearlman.<sup>14</sup> In the previous work, a variety of binding energy estimating methods were evaluated with these ligands, including scoring functions implemented in molecular docking, OWFEG, TI, and MD-PB/SA. As expected, MD-PB/

**Table 1. Structure and Activities of 16 Ligands in the p38 MAP Kinase Congeneric Data Set**



no.	R <sup>1</sup>	R <sup>2</sup>	R <sup>3</sup>	expr (pIC <sub>50</sub> )
1	H	H	H	6.602
2	H	H	F	7.000
3	H	H	Me	5.854
4	H	Cl	Cl	6.097
5	H	Me	H	5.854
6	H	Me	Me	5.721
7	H	F	H	6.347
8	Me	H	H	6.699
9	H	Cl	F	6.301
10	H	Cl	H	6.553
11	Me	H	Cl	6.745
12	Br	H	H	6.602
13	Me	H	Me	6.577
14	OH	H	H	6.444
15	NH <sub>2</sub>	H	F	6.658
16	Cl	H	F	7.444

SA was shown inferior to robust TI and OWFEG but, surprisingly, was even worse than Dock Energy Score in most cases. It is very interesting to reevaluate MD-PB/SA with this data set and figure out the potential problem.

For the starting conformation of receptor–ligand complex, we referred to the crystal structure of p38 MAP kinase in complex with a small molecular inhibitor **094** (PDB ID 1OYU), which shows much similarity to 16 cognates in this study. We generated the initial binding poses with molecular docking, then minimized the ligand structure in context of receptor binding pocket, and rescored the complex with MM-GB/SA. At last, we performed MD simulation of the binding site (12 Å around ligand) with an explicit solvent model and calculated binding free energy with the MD-PB/SA method. The above sequential operations were generally applied as a hierarchical strategy due to the good balance between efficiency and accuracy, which has been confirmed by our previous work.<sup>21–23</sup>

As a result, we obtained both structural information and binding free energies for 16 cognates. As to the simulation, it seems reasonable that a relatively small root-mean-square deviation (RMSD) (1–2 Å) was observed for the scaffold when we compared simulated results with reference crystal structure (PDB ID 1OYU) (Figure 1A). The favorable interactions between native ligand and receptor, including hydrogen bonds with backbone of His107 and Met109 in the hinge region as well as hydrophobic interaction with specific binding pocket (Figure 1A), were well conserved in the simulation results for 16 cognates.

As to the estimation, all the components of MD-PB/SA binding free energy are shown in Table 2. When we compared the calculated  $\Delta G$  with experimental data (pIC<sub>50</sub>), a good correlation with R<sup>2</sup> value as high as 0.50 was obtained (Figure 1B). For convenience of comparing, we also determined the predictive index (PI) for 16 cognates, which was shown to be 0.03–0.45 in a previous report.<sup>14</sup> Consistent with the R<sup>2</sup>

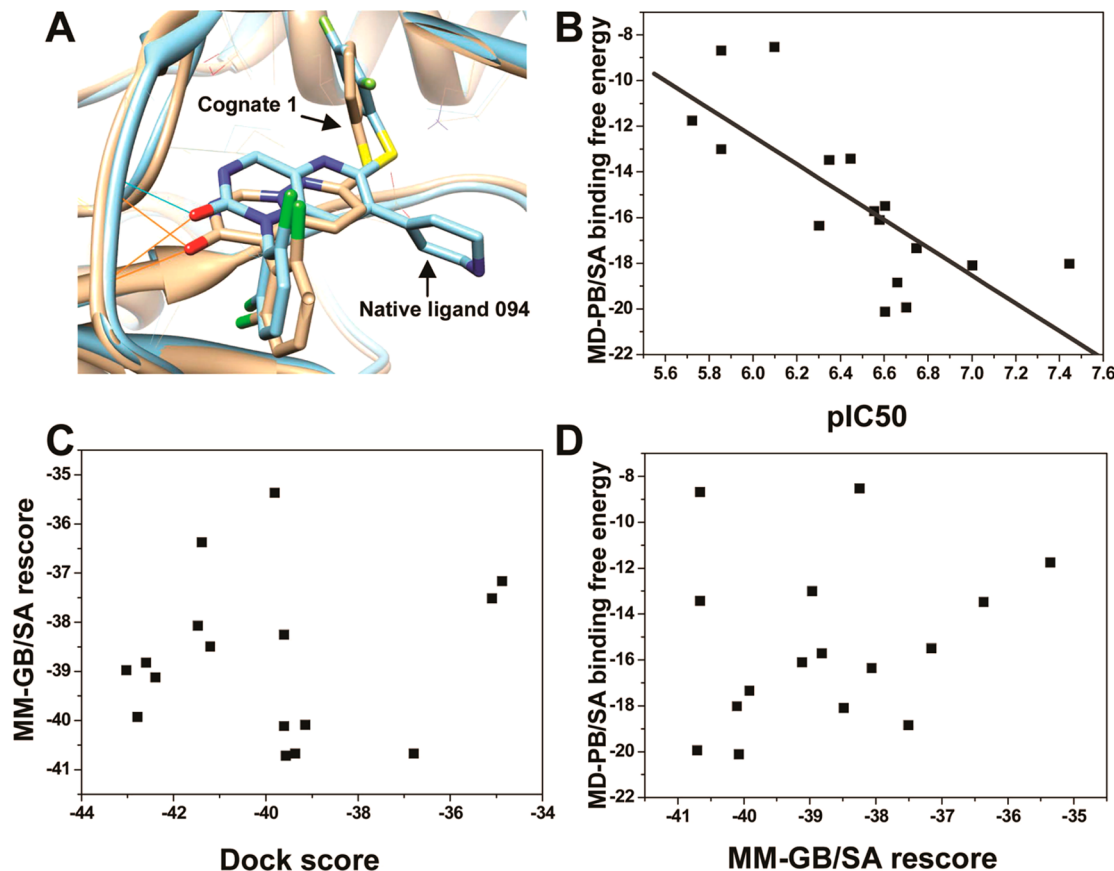


**Figure 1.** Structure and scores of p38 MAP kinase congeneric data set. (A) Superimposed calculated structure (cognate 1) and crystal structure (native inhibitor 094) with hydrogen bonds presented in cyan and orange lines. (B) Correlation between MD-PB/SA calculated binding free energy and experimental inhibition ability. (C) Comparison of dock score and MM-GB/SA rescore for 16 cognates. (D) Comparison of MM-GB/SA rescore and MD-PB/SA calculated free energy for 16 cognates.

**Table 2. Components of Binding Free Energy Calculated by MD-PB/SA**

no.	$\Delta V_{mm}$	$\Delta \Delta G_{\text{nonpolar}}$	$\Delta \Delta G_{\text{elec}}$	$\Delta H$	$T \Delta S$	$\Delta G$
1	-59.21(3.16) <sup>a</sup>	-5.15(0.07)	29.24(2.39)	-35.13(2.79)	-19.65(3.10)	-15.48
2	-63.39(2.92)	-5.29(0.05)	29.58(1.91)	-39.09(2.38)	-21.01(5.08)	-18.08
3	-58.85(3.09)	-5.46(0.05)	32.72(2.25)	-31.59(2.80)	-22.91(5.03)	-8.68
4	-59.06(3.02)	-5.40(0.07)	31.71(2.52)	-32.75(2.89)	-24.23(3.67)	-8.52
5	-62.43(3.10)	-5.41(0.09)	32.20(2.47)	-35.64(2.72)	-22.64(4.34)	-13
6	-58.54(3.11)	-5.62(0.06)	31.78(2.55)	-32.38(3.32)	-20.64(2.88)	-11.74
7	-59.20(2.65)	-5.43(0.06)	31.18(2.73)	-33.45(3.21)	-19.98(4.44)	-13.47
8	-63.70(2.84)	-5.42(0.06)	31.31(2.23)	-37.81(2.96)	-17.88(6.93)	-19.93
9	-63.38(3.22)	-5.42(0.08)	31.51(2.47)	-37.30(2.51)	-20.95(3.86)	-16.35
10	-59.76(3.44)	-5.30(0.07)	29.27(2.02)	-35.79(3.12)	-20.08(5.00)	-15.71
11	-65.51(2.80)	-5.61(0.06)	33.17(2.91)	-37.95(3.30)	-20.62(4.85)	-17.33
12	-64.61(2.91)	-5.39(0.05)	31.36(2.20)	-38.64(2.69)	-18.53(4.26)	-20.11
13	-66.41(3.36)	-5.57(0.06)	34.63(2.31)	-37.35(3.29)	-21.25(4.39)	-16.1
14	-67.59(4.11)	-5.32(0.05)	41.41(3.01)	-31.50(3.47)	-18.08(3.94)	-13.42
15	-71.45(4.43)	-5.19(0.05)	37.05(3.19)	-39.59(3.46)	-20.76(4.20)	-18.83
16	-59.30(2.89)	-5.38(0.06)	26.78(2.41)	-37.90(2.54)	-19.88(3.55)	-18.02

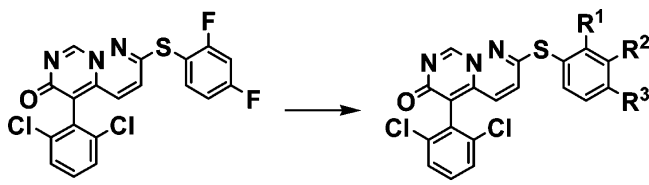
<sup>a</sup>All energies are in kilocalories per mole. Energy values in parentheses are the associated root-mean-squared deviations.

statistic, a promising result was shown with PI value as high as 0.79 for free energy and 0.73 for enthalpy (Table 3). It is also worth noting that counting the contribution of entropy only slightly improves the PI value from 0.73 to 0.79; however, the computational cost for entropy is much more than enthalpy alone.

**Table 3. Predictability of Different Methods for p38 MAP Kinase Congeneric Data Set**

method	DOCK	MM-GB/SA	FEP	MD-PB/SA	
				$\Delta H$	$\Delta G$
PI	-0.13	0.30	0.66	0.73	0.79

Table 4. Results of FEP Calculation for p38 MAP Kinase Congeneric Data Set



Reference state A				State B			
no.	disturb	$\Delta G$ (kcal/mol)	expr (kcal/mol)	no.	disturb	$\Delta G$ (kcal/mol)	expr (kcal/mol)
1	Ph	2.28	1.98	9	<i>m</i> -Cl, <i>p</i> -F	3.42	2.40
2	<i>p</i> -F	1.31	1.44	10	<i>m</i> -Cl	3.86	2.05
3	<i>p</i> -CH <sub>3</sub>	2.71	3.01	11	<i>o</i> -CH <sub>3</sub> , <i>p</i> -Cl	2.03	1.79
4	<i>m</i> -Cl, <i>p</i> -Cl	2.86	2.68	12	<i>o</i> -Br	5.44	1.98
5	<i>m</i> -CH <sub>3</sub>	4.79	3.01	13	<i>o</i> -CH <sub>3</sub> , <i>p</i> -CH <sub>3</sub>	4.13	2.02
6	<i>m</i> -CH <sub>3</sub> , <i>p</i> -CH <sub>3</sub>	4.30	3.19	14	<i>o</i> -OH	4.13	2.20
7	<i>m</i> -F	2.78	2.33	15	<i>o</i> -NH <sub>2</sub> , <i>p</i> -F	4.01	1.91
8	<i>o</i> -CH <sub>3</sub>	3.97	1.85	16	<i>o</i> -Cl, <i>p</i> -F	0.56	0.83

Table 5. Results of MD-PB/SA Calculation for p38 MAP Kinase Diverse Data Set with a Hierarchical Strategy

no.	MD-PB/SA ( $\Delta H$ )	MD-PB/SA ( $T\Delta S$ )	MD-PB/SA ( $\Delta G$ )	expr (pIC <sub>50</sub> )	RMSD(Å)
1	-11.29 (3.89) <sup>a</sup>	-17.00 (4.33)	5.71	7.32	4.176
2	-20.68 (3.33)	-16.97 (4.07)	-3.71	6.8	5.817
3	-8.37 (3.13)	-19.35 (4.56)	10.98	7.72	1.986
4	-20.11 (2.84)	-19.63 (4.83)	-0.48	7.6	2.603
5	-21.57 (2.54)	-19.09 (4.45)	-2.48	5.3	7.000
6	-28.47 (3.96)	-20.58 (5.70)	-7.89	8.58	3.153
7	-8.25 (2.94)	-24.51 (5.07)	16.26	9.89	7.738
8	-26.15 (2.58)	-22.91 (4.06)	-3.24	8.37	1.083
9	-20.52 (3.48)	-22.15 (5.12)	1.63	9.13	1.603
10	-14.09 (2.50)	-18.71 (3.60)	4.62	3	3.529
11	-22.15 (2.23)	-17.39 (4.19)	-4.76	4.46	3.095
12	-10.34 (2.31)	-13.56 (2.39)	3.22	3	4.204
13	-22.19 (2.78)	-21.37 (3.88)	-0.82	4.36	2.691
14	-8.61 (3.26)	-20.76 (3.15)	12.15	5.82	9.495
15	-11.42 (4.03)	-23.50 (4.45)	12.08	5.22	9.406
16	-25.56 (2.59)	-19.81 (6.63)	-5.75	8.3	1.000
17	-15.07 (3.70)	-20.42 (3.12)	5.35	6.16	5.367
18	-39.68 (3.05)	-22.53 (5.25)	-17.15	8.05	3.474
19	-24.47 (3.23)	-25.14 (6.04)	0.67	7.89	9.410

<sup>a</sup>All energies in kilocalories per mole. Energy values in parentheses are the associated root-mean-squared deviations.

With confidence of MD-PB/SA performance, we turned back to the comparison between different methods. Interestingly, there is no relationship between docking and MM-GB/SA scores (Figure 1C) while a positive correlation existing between MM-GB/SA and MD-PB/SA binding energies (Figure 1D). Molecular docking has been widely used in the virtual screening of large compound libraries due to the fast performance. However, the high efficiency was generally achieved by sacrificing the accuracy of scoring function. Components contributing to ligand–receptor interaction are neglected or largely simplified, such as solvent effect, receptor flexibility, entropy contribution, and so on. Fully considering these determinants would definitely make fast evaluation of large library unavailable. One alternative way is dividing the whole task into several dependent steps, which means we start with fast but approximate docking, then follow with moderate MM-GB/SA minimization and rescoring, and finally perform more accurate but expensive MD-PB/SA simulation and free energy calculation. The rationale of such strategy is based on the inference that as more physics-based determinants involved the

accuracy enhanced. In contrast to docking, both MM-GB/SA and MD-PB/SA methods consider solvent effects with an implicit solvent model, which explains the difference in the correlation between different methods (Figure 1C and D). Additionally, the best performance of MD-PB/SA in correlating with experimental data (Figure 1B) could be attributed to the full sampling of the energy landscape in MD simulation with the explicit solvent model, the more accurate PB method for estimating the polar contribution of solvent effects, and the consideration of entropy contributions.

Due to the similarity of 16 cognates, we performed free energy perturbation (FEP) calculations. The reference state “A” for all simulations was the molecule shown in Table 4. The binders “B” are all variants on the basic scaffold differing from the reference state only in relatively small substituents on the ring as shown and listed in Table 1. By disturbing the functional groups ( $R^1$ ,  $R^2$ , and  $R^3$ ) sequentially, we obtained the relative binding free energies for these ligands and compared them with experimental data (Table 4). From our results, it is shown that FEP is well established with its high predictability (PI value as

high as 0.66). In this case, it seems comparable between results of both FEP and MD-PB/SA; however, the computational cost of MD-PB/SA is much less than that of FEP.

**Study of p38 Diverse Data Set.** With encouraging results for 16 congeneric ligands, we expanded our study to diverse data set for p38 MAP kinase. A total number of 19 p38 MAP kinase inhibitors were collected from PDBbind database, all of which were characterized with clarified action modes from crystal structure and credible binding affinities (Table S1). To be consistent with the above work, we selected the same crystal structure (PDB ID 1OUY) as the starting model of receptor for the hierarchical calculations. The results of MD-PB/SA estimation are given in Table 5, which contains both estimated binding free energy and structural difference between simulated results and native pose from crystal structure.

Surprisingly, it is found that MD-PB/SA largely failed at this time (Table 6). Since structural diversity exists extensively in

**Table 6. Predictability of MD-PB/SA for p38 MAP Kinase Diverse Data Set**

method			all 19 ligands with superimposed poses	
	all 19 ligands with docking poses ( $\Delta H$ )	10 ligands with correct poses ( $\Delta H$ )	$\Delta H$	$\Delta G$
PI	0.21	0.41	0.51	0.38

the compound library and is more appreciated in the high throughput screening, we are interested to figure out why there is a huge difference in the performance of MD-PB/SA between congeneric and diverse data sets.

We first came back to the binding poses. As a result, it was found that large deviation (RMSD > 4 Å) existed between calculated and native poses (from crystal structure) for nine of the total ligands. For clarity, we discuss three different cases:

- (1) Calculation gave the correct binding pose close to the native structure. Taking ligand 3 as an example (Figure 2A and B), the RMSD values for small molecules between calculated and crystal structures were shown to be 2.008 (MM-GB/SA) and 1.986 (MD-PB/SA). Specifically, MD-PB/SA further improved the refined docking pose by rebuilding a lost hydrogen bond with the hinge region while maintaining other native interactions, including a hydrogen bond with conserved Lys53 and hydrophobic interaction with a specific pocket.
- (2) Calculation gave an incorrect binding pose far from the native structure. Taking ligand 7 as an example (Figure 2C and D), the RMSD values for small molecules between calculated and crystal structures were 7.957 (MM-GB/SA) and 7.738 (MD-PB/SA), respectively. This suggests MD-PB/SA could not correct the large deviation in the ligand pose and failed to predict the relative binding energy.
- (3) Calculation gave both correct and incorrect binding poses. Taking ligand 9 as an example (Figure 2E and F), based on results from docking and rescoring, MD-PB/SA distinguished the correct pose ( $\Delta G = -20.52$  kcal/mol) from the incorrect one ( $\Delta G = -14.44$  kcal/mol) by a favorable energy difference of more than 6 kcal/mol. However, when we compared results for different ligands, it is noted that even the less favorable score

(−14.44 kcal/mol) for the incorrect pose of **9** is still more favorable than the correct pose of **3** ( $\Delta G = -8.37$  kcal/mol). This suggests that there are limitations in MD-PB/SA in dealing with more complicated issues, such as distinguishing different poses for diverse ligands, which brings up great challenges to the current physics-based scoring function.

Interestingly, we noted that most of the incorrect binding poses could be easily excluded on the basis of well-established knowledge about kinase inhibitor, such as important hydrogen bond with hinge region, hydrophobic interaction with the specific pocket, and so on.<sup>24</sup> Then, as the second step, we excluded nine molecules with incorrect binding pose or large deviation from native structure (RMSD > 4 Å), and then, reevaluated the predictability of MD-PB/SA. As a result, we obtained an encouraging result of PI value as high as 0.41 for the remaining 10 ligands (Table 6). This validates the above inference that it is a problem with the starting structure that leads to the inaccuracy of MD-PB/SA prediction.

To further confirm this, we chose an alternative strategy for generating the starting structure for 19 ligands, which means we obtained the binding poses of 19 ligands by superimposing the native complex structure from crystal to the reference structure (1OUY), rather than by molecular docking. This ensures our starting model is very close to the native structure and thus provides a reasonable basis for predicting the action mode (Table S4). From our results, it is shown that MD-PB/SA predicts the relative binding energy very well for all the 19 ligands, with a PI value as high as 0.51 (Table 6). In addition, enthalpy estimation alone performs better than free energy in relating with the experimental affinities. This could be attributed to the much larger fluctuations of entropy than enthalpy during MD trajectories (Table 2 and 5), which could impair the stable prediction of MD-PB/SA protocol. Consistently, previous reports have also highlighted the largest variation for entropy estimation among the five individual energy terms of MD-PB/SA calculation.<sup>3,16</sup> On the other hand, entropy is also the term that has the most costs in both human and computational resources, especially regarding the necessity of collecting a large number of snapshots to achieve stable predictions, which makes the practical use almost forbidden. On these basis, it is suggested we neglect the entropy contribution in the lead discovery from virtual screening of large commercial library.

It is also worth noting that the predictability of enthalpy estimation in congeneric data set seems superior to that in diverse data set (PI value: 0.73 vs 0.51). This could be attributed to the well-known eliminating systematic errors in the former case, which consists of structurally similar compounds based on the same scaffold. We can also find some clues from the observation that other scoring functions, such as MM-GB/SA implemented in PLOP, similarly show much better predictability in the congeneric series (PI value: 0.30 vs −0.09).

**Virtual Screening of p38 Inhibitor.** After evaluation of MD-PB/SA with p38 ligands, we determined to apply it to the practice of lead discovery for its well-established role as a promising target for inflammation treatment. Consistent with the above studies, we implemented MD-PB/SA in the hierarchical virtual screening pipeline, and aimed at the in-house library containing 100 413 diverse drug-like small molecular compounds, which were collected from commercial

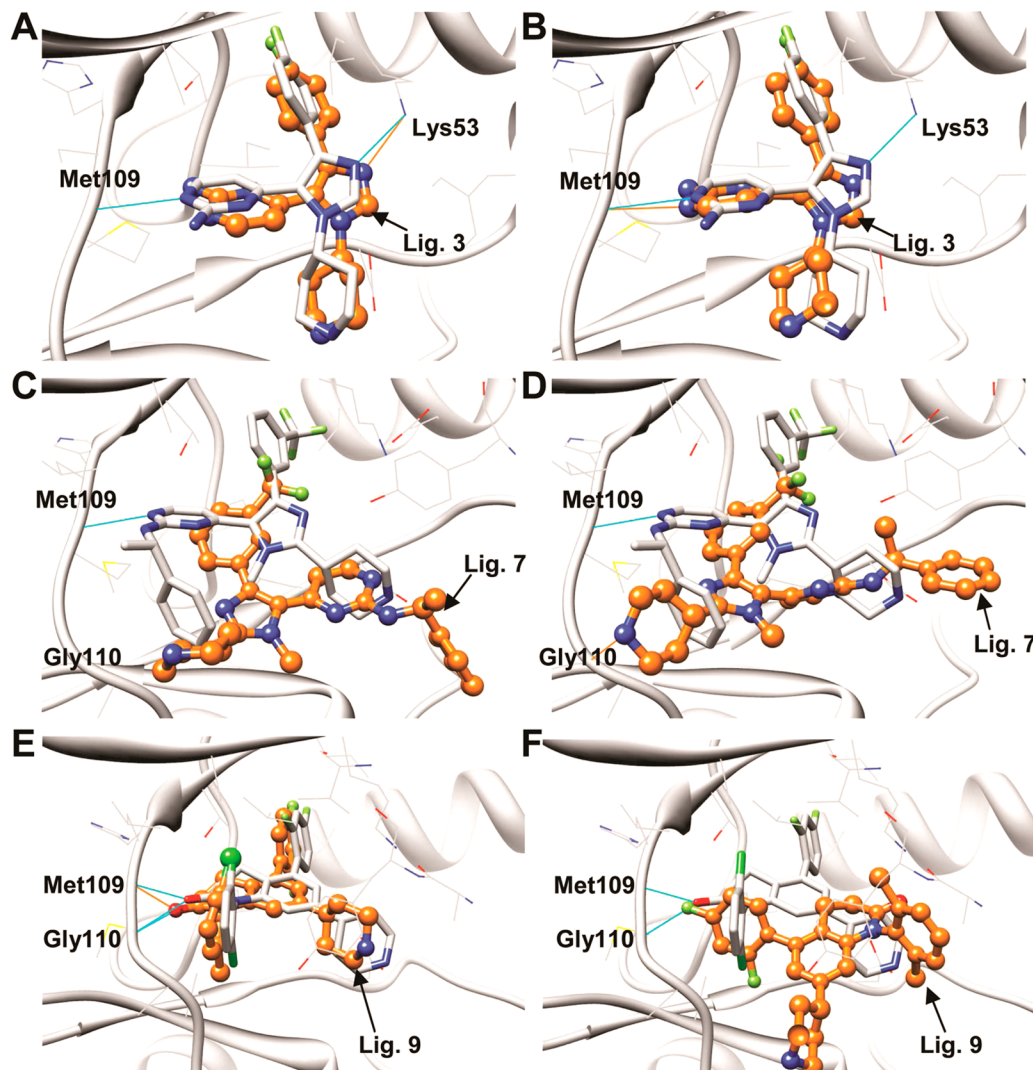


**Figure 2.** Comparison of crystal structure and calculation results for exemplified ligands. Crystal structure was shown in light gray color and represented in sticks and wires for the ligand and residues, respectively. The calculated structure for ligand was shown in orange color and represented in ball-and-stick. Hydrogen bonds were shown in cyan and orange lines. (A and B) Superimposed crystal structure with refined docking pose (A) and MD-PB/SA simulated structure (B) for ligand 3, respectively. (C and D) Superimposed crystal structure with refined docking pose (C) and MD-PB/SA simulated structure (D) for ligand 7, respectively. (E and F) Superimposed crystal structure with correct (E) and incorrect (F) binding poses from MD-PB/SA simulation for ligand 9.

databases, such like ChemDiv and Specs. To exclude interference of artificial poses, we developed structural filters to assist physics-based scoring function based on well-established knowledge about kinase inhibitor, including (1) hydrogen bond with hinge region of protein kinase, including carbonyl group of His107 or amide group of Met109 or Gly110 and (2) hydrophobic interaction with the specific pocket surrounded by residues Val38, Leu75, Ile84, and Leu104. These were used as structural filters during the process of hierarchical virtual screening and assisted at each step to reduce the number of candidates by excluding those highly ranked molecules but with unlikely binding poses. In other words, only the molecules meeting both hydrogen bond(s) and hydrophobic interactions could survive from the evaluation.

The results of HVS is shown in Figure 3A. We first generated a total number of 358 954 potential binding poses for 100 413 compounds. After the first filtering, only 199 597 molecules survived and were minimized in the context of binding site as well as rescored with MM-GB/SA method. A total of 20 381

molecules with favorable binding energies were submitted to the second filtering, from which we selected the top 500 different compounds for the next MD-PB/SA calculation. After binding energy estimation and structural filtering, 54 compounds with both favorable binding energies and qualified structure finally survived, from which the top-ranked 7 compounds were selected as candidates (Figure 3B). The predicted binding modes for these candidates were shown in Figure S1.

For the experimental validation, we first examined the inhibition of kinase activity at single dose of concentration ( $50 \mu\text{M}$ ). As a result, five of seven candidates showed activities (1, 2, 3, 4, 5) and three compounds with significant inhibition more than 50% (1, 3, 4) (Figure 3C), which were selected as leads. On this basis, we further determined the dose-response curves for each of them and obtained the  $\text{IC}_{50}$  values of  $30 \pm 0.7$ ,  $5.9 \pm 0.2$ , and  $38.6 \pm 0.4 \mu\text{M}$  for 1, 3, 4, respectively. To explore the novelty, we first performed the SEA (Similarity Ensemble Approach) analysis on the above three hits. From the

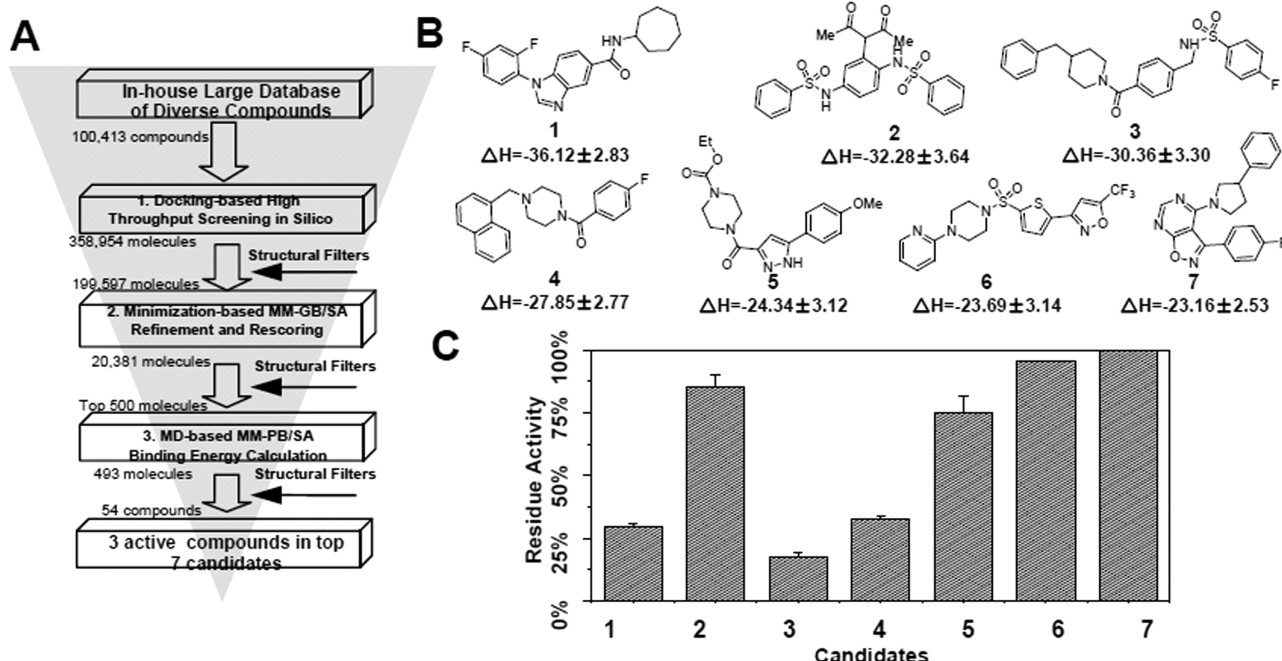


**Figure 3.** Results of hierarchical virtual screening against p38 MAP kinase. (A) Flowchart of hierarchical virtual screening. (B) Structure of seven candidates survived from hierarchical virtual screening. (C) Kinase activity assay results for seven candidates.

results (Table S7–S9), it is shown that although p38 MAPK was identified as the potential target for hit 1 with a rank as high as 16th; however, for hit 3 and 4, p38 was not found in the ranking list of top 50 potential targets, which suggests the high novelty in these two compounds. In addition, we compared the structural similarity of 3 (as the most potent hit) with other well-established p38 inhibitors (Table S10). It is shown that the calculated Tc value (Tanimoto coefficient) is less than 0.25 (Table S10), which confirmed the structural novelty of our hit.

Encouraged by the above results, we also tried other different strategies. First, we performed hierarchical virtual screening without structural filters. In this way, we differentiated the promising compounds from the inferior ones merely by the judgment of physics-based scoring function, such as the basic scoring function in molecular docking, MM-GB/SA in PLOP and MM-PB/SA in MD-PB/SA protocols. Specifically, we generated 358 954 different binding poses for a total number of 100 413 compounds. To reduce the computational costs, we selected the top 5% molecules based on docking scores and put them into MM-GB/SA rescoring which resulted in 10 214 molecules with favorable binding energies. For more consuming MD-PB/SA calculation, we selected the top 1% of compounds based on MM-GB/SA scores. For the experimental validation, we selected the top seven candidates without any inspective inference (compounds 1'–7', Figure S2). As a result, none of them was identified as active inhibitor. When we went back to the predicted binding poses (Figure S2), it is interesting to find that all these candidates were suffering the lost of either hydrogen bonds with hinge region or hydrophobic interaction with the specific pocket. This is consistent with our previous observation that there is a limitation for MD-PB/SA in differentiating different poses of diverse ligands.

To determine the role of structural filters in identifying active binders, we also selected the top seven candidates (compounds 1'–7', Figure S3) straight from the structurally filtered docking results. None of these candidates was shown to be active, even

at concentrations as high as 50  $\mu$ M (Figure S3). Interestingly, when we performed MD-PB/SA calculations on these seven candidates, none of them showed a favorable binding energy lower than  $-24$  kcal/mol. Taken together, it is suggested that both structural filter and advanced physics-based scoring function, such as implemented in MD-PB/SA, make great contributions to the final result.

**Study of HIV-1 RT and NA Diverse Data Sets.** According to the above results, we were confident in the performance of MD-PB/SA in p38 ligand binding estimation. To further extend our study, we also evaluated the predictability with other druggable targets, including HIV-1 RT and NA protein. We collected 18 and 13 diverse ligands from PDBbind database for each target, which share both qualified structural information and credible binding affinity data (Table S2 and S3). In addition, the activity of these compounds expands a large scale of  $pIC_{50}$  values. Learning from previous experience, (1) we adopted the water sphere model with a radius of 30 Å to fully cover the binding pocket; (2) we generated the starting model for the ligands by superimposing crystal structures, which ensures the accuracy of initial binding poses; (3) we predicted the relative binding affinities with enthalpy rather than entropy contribution. On this basis, satisfied results were obtained with the PI value of 0.59 and 0.73 for HIV-1 RT and NA, respectively, which proves the general validity of MD-PB/SA method. The calculated binding energies as well as RMSD values for HIV-1 RT and NA protein are shown in the Supporting Information (Table S5 and S6).

## CONCLUSION

In the present study, we reported a critical evaluation and practical application of MD-PB/SA in the routinely applied hierarchical virtual screening for lead discovery. As a result, we found the predictability could be significantly improved by adopting water sphere model with radius as large as 30 Å and accurate starting pose for the ligand. However, there is a

limitation for MD-PB/SA in distinguishing different binding poses of different ligands when huge diversity exists in structure. By combining a physics-based scoring function with a knowledge-based structural filter, we improved the predictability and validated the practical use of MD-PB/SA in lead discovery by identifying novel inhibitors of p38 MAP kinase. Additionally, we confirmed the general validity of MD-PB/SA by expanding our study to HIV-1 RT and NA protein.

## MATERIALS AND METHODS

**System Preparation.** Crystal structures with high quality were selected for p38 MAP kinase (PDB ID 1OUY), HIV-1 RT (PDB ID 1UWB), and NA protein (PDB ID 1F8B) as the starting model, respectively. The cognate data set for p38 MAP kinase consisting of a set of 16 congeneric ligands was collected from previous reports by Pearlman while other three diverse data sets for p38 MAP kinase, HIV-1 RT, and NA were collected from the PDBBind database,<sup>25</sup> with structural information and binding affinities shown in Tables S1–S3.

**Molecular Docking.** As the first step of hierarchical virtual screening (HVS),<sup>21</sup> fast molecular docking was performed with DOCK 3.5.54, a flexible-ligand method that uses a force-field-based scoring function composed of van der Waals and electrostatic interaction energies corrected for ligand desolvation.<sup>26–28</sup> All the compounds in the library were prepared in db format with ZINC protocol.<sup>29</sup> Binding site residues were identified within 12 Å of native ligand from cocrystal structure, and the solvent-accessible molecular surface<sup>30</sup> was calculated with the program DMS<sup>31</sup> using a probe radius of 1.4 Å. Receptor-derived spheres were generated with the program SPHGEN<sup>32</sup> while the ligand-derived spheres were from the positions of the heavy atoms of ligand. Four sets of grids were generated: an excluded volume grid using DISTMAP,<sup>26</sup> a united atom AMBER-based van der Waals potential grid using CHEMGRID,<sup>26</sup> an electrostatic potential grid using DelPhi,<sup>33</sup> and a solvent occlusion map using the program SOLVMAP.<sup>34</sup> Ligand conformations were scored on the basis of the total energy after 25 steps of rigid-body minimization, which is the sum of electrostatic and van der Waals interaction energies, corrected by the partial ligand desolvation energy.

**MM-GB/SA Rescore.** As the second step of HVS, MM-GB/SA refinement and rescoring was performed using Protein Local Optimization Program (PLOP).<sup>35–37</sup> This approach accounts for more accurate and efficient calculations of ligand–protein interaction energies, the ligand/receptor desolvation, and to a lesser extent, ligand strain energies. Briefly, the docked protein–ligand complex and ligand were submitted to multiscale Truncated Newton energy minimization in all-atom OPLS force field and Generalized Born solvent as described previously.<sup>38–40</sup> The protein structure used in the docking was used for rescoring. Hydrogen atoms were added in standard geometries as defined by the all-atom OPLS force field.<sup>41,42</sup> The protein was kept rigid during ligand–protein complex minimization in this work. The binding energy ( $E_{\text{bind}} = E_{\text{R}^*\text{L}} - E_{\text{L}} - E_{\text{R}}$ ) was calculated by subtracting the energies of the optimized free ligand in solution ( $E_{\text{L}}$ ) and the free protein in solution ( $E_{\text{R}}$ ) from the optimized ligand–protein complex's energy in solution ( $E_{\text{R}^*\text{L}}$ ).

**MD-PB/SA Calculation.** As the final step of HVS, MD-PB/SA calculation was carried out using AMBER10.0 suite.<sup>43</sup> The AMBER99SB force field<sup>44</sup> was applied for receptor and the general Amber force field (GAFF)<sup>45</sup> for the ligands. ANTECHAMBER was used for calculating the AM1-BCC

charges of ligands. All system setups were performed in TLEAP module. Simulations were carried out using the SANDER module. For each complex, three stages of minimization were performed in gas phase, followed by the addition of a 30 Å water cap based on the geometric center of binding site. After 200 ps of equilibration of solvents, a production run of 5 ns was performed on the whole system at 300 K with a time step of 2.0 fs. All residues including solvents beyond 12 Å of ligand are fully frozen. 100 snapshots were evenly extracted from last 1 ns simulation. The interaction energy between receptor and ligand as well as internal energy was calculated with SANDER module. As to the solvation energy, polar contribution is calculated using PBSA<sup>46</sup> with PARSE radii while nonpolar part is estimated proportional to the solvent-accessible surface area.<sup>47</sup> All the computational tasks were performed on our Linux clusters and managed with the scheduling system SGE.

**Free Energy Perturbation Calculation.** In order to calculate the free-energy difference between the reference state "A" and variant state "B", the free energy perturbation (FEP) method was used.<sup>48</sup> To construct the initial "B" states, each of 16 cognates was first docked into p38 active site (PDB ID 1OUY) with DOCK3.5.54, which was followed by MM-GB/SA minimization and rescoring with PLOP. For FEP simulation, the reaction path between two thermodynamic states 0 (reference state A) and 1 (variant state B) is divided into  $N$  nonphysical intermediate windows according to the coupling parameter  $\lambda$ , which varies from 0 to 1 accordingly (Formula 3):

$$\begin{aligned}\Delta G_{0 \rightarrow 1} &= G(\lambda_1) - G(\lambda_0) \\ &= -k_B T \sum_{k=1}^{N-1} \ln \left\langle \exp \left[ -\frac{U(x, \lambda_{k+1}) - U(x, \lambda_k)}{k_B T} \right] \right\rangle_{\lambda_k}\end{aligned}\quad (3)$$

where  $\Delta G$  is the free energy difference between the two states (0 and 1),  $k_B$  is the Boltzmann constant,  $T$  is the temperature (300 K), and  $U$  is the potential energy of the system, which is dependent on the Cartesian coordinates of each window and the coupling parameter. In each FEP simulation, the reaction path was divided into 6 and 15 windows for Coulombic and van der Waals interactions, respectively. An initial equilibration simulation of 20 ps was followed by 100 ps production run and data collection. Postprocessing was performed by WHAM.<sup>49–51</sup>

**Reagents and Chemicals.** Chromatographic resins, NI-NTA-Agarose, and Superdex 75 were purchased from GE Healthcare (Piscataway, NJ). The DNA sequences encoding the human mitogen-activated protein kinase 14 (hMAPK14) (UniprotKB/Swiss-prot: Q16539) and the human mitogen-activated protein kinase kinase 6 (hMKK6) (UniprotKB/Swiss-prot: P52564) were purchased from OpenBiosystems (Huntsville, AL). The S207D/T211D mutagenesis of hMKK6 was carried out with the Site-Directed Mutagenesis Kit from Transgen, which generated the product of hMKK6DD. The in-house library for virtual screening contains more than 100 000 diverse compounds with drug-like properties, which were collected from large commercial libraries (such as ChemDiv, Specs).

**Kinase Activity Assay.** Inactive hMAPK14 was activated by constitutively active hMKK6DD at 30 °C. Then enzymatic activity assay was performed in 384-well assay plates with a total volume of 10 μL. Kinase reactions were carried out according to the manual using the Z'-LYTE kinase assay kit (Ser/Thr 15 peptide), a FRET(fluorescence resonance energy transfer) based method provided by Invitrogen Corporation. Briefly, the

reaction system contains 50 mM HEPES (pH 7.5), 10 mM MgCl<sub>2</sub>, 1 mM EGTA, 0.01% Brij-35, and 0.1% Triton X-100. Activated hMAPK14 (110 nM of final concentration) was preincubated with compounds or DMSO control for 15 min at room temperature. Phosphorylation reactions were initiated by the addition of 2 μM peptide substrate and 100 μM ATP. After 1 h at room temperature, 2.5 μL development reagents were added to stop the reaction and cleave nonphosphorylated peptide substrate. After 1 h at room temperature, development reactions were then quenched with 2.5 μL stop reagents. The coumarin and fluorescein emission signals (excitation at 400 nm while emission at 445 and 520 nm, respectively) were measured with the Beckman Coulter paradigm detection platform.

## ASSOCIATED CONTENT

### Supporting Information

Predicted binding modes for candidates from hierarchical VS with structural filters; results of hierarchical virtual screening without structural filters as well as molecular docking combined with structural filtering; structure and affinities of 19 diverse ligands for p38 MAP kinase; structure and affinities of 18 diverse ligands for HIV-1 RT; structure and affinities of 13 diverse ligands for NA protein; results of MD-PB/SA for diverse data sets of p38, HIV-1 RT, and NA protein; results of SEA search for positive hits; structural comparison of hit 3 with well-established p38α inhibitors. This material is available free of charge via the Internet at <http://pubs.acs.org>.

## AUTHOR INFORMATION

### Corresponding Author

\*Phone: 86-10-80726688. E-mail: wangyanli@nibs.ac.cn.

### Notes

The authors declare no competing financial interest.

## ABBREVIATIONS

MD, molecular dynamics; RMSD, root-mean-square deviation; MM, molecular-mechanics; GB/SA, generalized born surface area; MM-PB/SA, molecular-mechanics Poisson–Boltzmann surface area; PLOP, protein local optimization program; GAFF, general Amber force field; HIV, human immunodeficiency virus; NA, neuraminidase; RMSD, root-mean-square deviation

## REFERENCES

- (1) Kuhn, B.; Gerber, P.; Schulz-Gasch, T.; Stahl, M. Validation and use of the MM-PBSA approach for drug discovery. *J. Med. Chem.* **2005**, *48*, 4040–4048.
- (2) Kollman, P. A.; Massova, I.; Reyes, C.; Kuhn, B.; Huo, S.; Chong, L.; Lee, M.; Lee, T.; Duan, Y.; Wang, W.; Donini, O.; Cieplak, P.; Srinivasan, J.; Case, D. A.; Cheatham, T. E., 3rd Calculating structures and free energies of complex molecules: combining molecular mechanics and continuum models. *Acc. Chem. Res.* **2000**, *33*, 889–897.
- (3) Hou, T.; Wang, J.; Li, Y.; Wang, W. Assessing the performance of the MM/PBSA and MM/GBSA methods. 1. The accuracy of binding free energy calculations based on molecular dynamics simulations. *J. Chem. Inf. Model.* **2011**, *51*, 69–82.
- (4) Hou, T.; Wang, J.; Li, Y.; Wang, W. Assessing the performance of the molecular mechanics/Poisson Boltzmann surface area and molecular mechanics/generalized Born surface area methods. II. The accuracy of ranking poses generated from docking. *J. Comput. Chem.* **2011**, *32*, 866–877.
- (5) Xu, L.; Sun, H.; Li, Y.; Wang, J.; Hou, T. Assessing the performance of MM/PBSA and MM/GBSA methods. 3. The impact of force fields and ligand charge models. *J. Phys. Chem. B* **2013**, *117*, 8408–8421.
- (6) Rastelli, G.; Del Rio, A.; Degliesposti, G.; Sgobba, M. Fast and accurate predictions of binding free energies using MM-PBSA and MM-GBSA. *J. Comput. Chem.* **2010**, *31*, 797–810.
- (7) Srivastava, H. K.; Sastry, G. N. Molecular dynamics investigation on a series of HIV protease inhibitors: assessing the performance of MM-PBSA and MM-GBSA approaches. *J. Chem. Inf. Model.* **2012**, *52*, 3088–3098.
- (8) Kuhn, B.; Kollman, P. A. Binding of a diverse set of ligands to avidin and streptavidin: an accurate quantitative prediction of their relative affinities by a combination of molecular mechanics and continuum solvent models. *J. Med. Chem.* **2000**, *43*, 3786–3791.
- (9) Wang, J.; Morin, P.; Wang, W.; Kollman, P. A. Use of MM-PBSA in reproducing the binding free energies to HIV-1 RT of TIBO derivatives and predicting the binding mode to HIV-1 RT of efavirenz by docking and MM-PBSA. *J. Am. Chem. Soc.* **2001**, *123*, 5221–5230.
- (10) Mobley, D. L.; Dill, K. A. Binding of small-molecule ligands to proteins: "what you see" is not always "what you get". *Structure* **2009**, *17*, 489–498.
- (11) Sims, P. A.; Wong, C. F.; McCammon, J. A. A computational model of binding thermodynamics: the design of cyclin-dependent kinase 2 inhibitors. *J. Med. Chem.* **2003**, *46*, 3314–3325.
- (12) Okimoto, N.; Futatsugi, N.; Fuji, H.; Suenaga, A.; Morimoto, G.; Yanai, R.; Ohno, Y.; Narumi, T.; Taiji, M. High-performance drug discovery: computational screening by combining docking and molecular dynamics simulations. *PLoS Comput. Biol.* **2009**, *5*, e1000528.
- (13) Rastelli, G.; Degliesposti, G.; Del Rio, A.; Sgobba, M. Binding estimation after refinement, a new automated procedure for the refinement and rescoring of docked ligands in virtual screening. *Chem. Biol. Drug Des.* **2009**, *73*, 283–286.
- (14) Pearlman, D. A. Evaluating the molecular mechanics poisson-boltzmann surface area free energy method using a congeneric series of ligands to p38 MAP kinase. *J. Med. Chem.* **2005**, *48*, 7796–7807.
- (15) Genheden, S.; Ryde, U. Improving the Efficiency of Protein–Ligand Binding Free-Energy Calculations by System Truncation. *J. Chem. Theory Comput.* **2012**, *8*, 1449–1458.
- (16) Weis, A.; Katabzadeh, K.; Soderhjelm, P.; Nilsson, I.; Ryde, U. Ligand affinities predicted with the MM/PBSA method: dependence on the simulation method and the force field. *J. Med. Chem.* **2006**, *49*, 6596–6606.
- (17) Uciechowska, U.; Schemies, J.; Neugebauer, R. C.; Huda, E. M.; Schmitt, M. L.; Meier, R.; Verdin, E.; Jung, M.; Sippel, W. Thiobarbiturates as sirtuin inhibitors: virtual screening, free-energy calculations, and biological testing. *ChemMedChem.* **2008**, *3*, 1965–1976.
- (18) Kumar, A.; Ito, A.; Hirohama, M.; Yoshida, M.; Zhang, K. Y. Identification of sumoylation activating enzyme 1 inhibitors by structure-based virtual screening. *J. Chem. Inf. Model.* **2013**, *53*, 809–820.
- (19) Chen, Y.; Fang, L.; Peng, S.; Liao, H.; Lehmann, J.; Zhang, Y. Discovery of a novel acetylcholinesterase inhibitor by structure-based virtual screening techniques. *Bioorg. Med. Chem. Lett.* **2012**, *22*, 3181–3187.
- (20) Venken, T.; Krnavek, D.; Munch, J.; Kirchhoff, F.; Henklein, P.; De Maeyer, M.; Voet, A. An optimized MM/PBSA virtual screening approach applied to an HIV-1 gp41 fusion peptide inhibitor. *Proteins* **2011**, *79*, 3221–3235.
- (21) Cao, R.; Liu, M.; Yin, M.; Liu, Q.; Wang, Y.; Huang, N. Discovery of novel tubulin inhibitors via structure-based hierarchical virtual screening. *J. Chem. Inf. Model.* **2012**, *52*, 2730–2740.
- (22) Li, W.; Wan, X.; Zeng, F.; Xie, Y.; Wang, Y.; Zhang, W.; Li, L.; Huang, N. More than just a GPCR ligand: structure-based discovery of thioridazine derivatives as Pim-1 kinase inhibitors. *MedChemComm* **2014**, *5*, 507–511.
- (23) Wan, X.; Zhang, W.; Li, L.; Xie, Y.; Li, W.; Huang, N. A New Target for an Old Drug: Identifying Mitoxantrone as a Nanomolar

- Inhibitor of PIM1 Kinase via Kinome-Wide Selectivity Modeling. *J. Med. Chem.* **2013**, *56*, 2619–2629.
- (24) Ghose, A. K.; Herbertz, T.; Pippin, D. A.; Salvino, J. M.; Mallamo, J. P. Knowledge based prediction of ligand binding modes and rational inhibitor design for kinase drug discovery. *J. Med. Chem.* **2008**, *51*, 5149–5171.
- (25) Wang, R.; Fang, X.; Lu, Y.; Yang, C. Y.; Wang, S. The PDBbind database: methodologies and updates. *J. Med. Chem.* **2005**, *48*, 4111–4119.
- (26) Meng, E. C.; Shoichet, B. K.; Kuntz, I. D. Automated docking with grid-based energy evaluation. *J. Comput. Chem.* **1992**, *13*, 505–524.
- (27) Lorber, D. M.; Shoichet, B. K. Hierarchical docking of databases of multiple ligand conformations. *Curr. Top Med. Chem.* **2005**, *5*, 739–749.
- (28) Wei, B. Q.; Baase, W. A.; Weaver, L. H.; Matthews, B. W.; Shoichet, B. K. A model binding site for testing scoring functions in molecular docking. *J. Mol. Biol.* **2002**, *322*, 339–355.
- (29) Irwin, J. J.; Shoichet, B. K. ZINC—a free database of commercially available compounds for virtual screening. *J. Chem. Inf. Model* **2005**, *45*, 177–182.
- (30) Connolly, M. L. Solvent-accessible surfaces of proteins and nucleic acids. *Science* **1983**, *221*, 709–713.
- (31) Ferrin, T. E.; Huang, C. C.; Jarvis, L. E.; Langridge, R. The MIDAS display system. *J. Mol. Graph. Model* **1988**, *6*, 13–27.
- (32) Kuntz, I. D.; Blaney, J. M.; Oatley, S. J.; Langridge, R.; Ferrin, T. E. A geometric approach to macromolecule-ligand interactions. *J. Mol. Biol.* **1982**, *161*, 269–288.
- (33) Nicholls, A.; Honig, B. A rapid finite difference algorithm, utilizing successive over-relaxation to solve the Poisson–Boltzmann equation. *J. Comput. Chem.* **1991**, *12*, 435–445.
- (34) Mysinger, M. M.; Shoichet, B. K. Rapid context-dependent ligand desolvation in molecular docking. *J. Chem. Inf. Model* **2010**, *50*, 1561–1573.
- (35) Jacobson, M. P.; Kaminski, G. A.; Friesner, R. A.; Rapp, C. S. Force Field Validation Using Protein Side Chain Prediction. *J. Phys. Chem. B* **2002**, *106*, 11673–11680.
- (36) Jacobson, M. P.; Pincus, D. L.; Rapp, C. S.; Day, T. J.; Honig, B.; Shaw, D. E.; Friesner, R. A. A hierarchical approach to all-atom protein loop prediction. *Proteins* **2004**, *55*, 351–367.
- (37) Li, X.; Jacobson, M. P.; Friesner, R. A. High-resolution prediction of protein helix positions and orientations. *Proteins* **2004**, *55*, 368–382.
- (38) Huang, N.; Kalyanaraman, C.; Irwin, J. J.; Jacobson, M. P. Physics-based scoring of protein-ligand complexes: enrichment of known inhibitors in large-scale virtual screening. *J. Chem. Inf. Model* **2006**, *46*, 243–253.
- (39) Huang, N.; Kalyanaraman, C.; Bernacki, K.; Jacobson, M. P. Molecular mechanics methods for predicting protein-ligand binding. *Phys. Chem. Chem. Phys.* **2006**, *8*, 5166–5177.
- (40) Huang, N.; Jacobson, M. P. Binding-site assessment by virtual fragment screening. *PLoS One* **2010**, *5*, e10109.
- (41) Jorgensen, W. L.; Maxwell, D. S.; Tirado-Rives, J. Development and Testing of the OPLS All-Atom Force Field on Conformational Energetics and Properties of Organic Liquids. *J. Am. Chem. Soc.* **1996**, *118*, 11225–11236.
- (42) Kaminski, G. A.; Friesner, R. A.; Tirado-Rives, J.; Jorgensen, W. L. Evaluation and Reparametrization of the OPLS-AA Force Field for Proteins via Comparison with Accurate Quantum Chemical Calculations on Peptides? *J. Phys. Chem. B* **2001**, *105*, 6474–6487.
- (43) Case, D. A.; Darden, T. A.; Cheatham, I. T. E.; Simmerling, C. L.; Wang, J.; Duke, R. E.; Luo, R.; Crowley, M.; Walker, R. C.; Zhang, W.; Merz, K. M.; Wang, B.; Hayik, S.; Roitberg, A.; Seabra, G.; Kolossváry, I.; Wong, K. F.; Paesani, F.; Vanicek, J.; Wu, X.; Brozell, S. R.; Steinbrecher, T.; Gohlke, H. AMBER 10; University of California, San Francisco, 2008.
- (44) Wang, J.; Cieplak, P.; Kollman, P. A. How well does a restrained electrostatic potential (RESP) model perform in calculating conformational energies of organic and biological molecules? *J. Comput. Chem.* **2000**, *21*, 1049–1074.
- (45) Wang, J.; Wolf, R. M.; Caldwell, J. W.; Kollman, P. A.; Case, D. A. Development and testing of a general amber force field. *J. Comput. Chem.* **2004**, *25*, 1157–1174.
- (46) Luo, R.; David, L.; Gilson, M. K. Accelerated poisson-boltzmann calculations for static and dynamic systems. *J. Comput. Chem.* **2002**, *23*, 1244–1253.
- (47) Sitkoff, D.; Sharp, K. A.; Honig, B. Accurate calculation of hydration free energies using macroscopic solvent models. *J. Phys. Chem.* **1994**, *98*, 1978–1988.
- (48) Zwanzig, R. W. High-Temperature Equation of State by a Perturbation Method. I. Nonpolar Gases. *J. Chem. Phys.* **1954**, *22*, 1420–1426.
- (49) Kumar, S.; Rosenberg, J. M.; Bouzida, D.; Swendsen, R. H.; Kollman, P. A. The weighted histogram analysis method for free-energy calculations on biomolecules. I. The method. *J. Comput. Chem.* **1992**, *13*, 1011–1021.
- (50) Kumar, S.; Rosenberg, J. M.; Bouzida, D.; Swendsen, R. H.; Kollman, P. A. Multidimensional free-energy calculations using the weighted histogram analysis method. *J. Comput. Chem.* **1995**, *16*, 1339–1350.
- (51) Roux, B. The calculation of the potential of mean force using computer simulations. *Comput. Phys. Commun.* **1995**, *91*, 275–282.